Molecular scale hydrodynamic theory of crystal nucleation and polycrystalline growth

Frigyes Podmaniczky [a,*], László Gránásy [a,b,*]

[a] *Institute for Solid State Physics and Optics, Wigner Research Centre for Physics, P O Box 49, H-1525 Budapest, Hungary*
[b] *BCAST, Brunel University, Uxbridge, Middlesex UB8 3PH, UK*

ARTICLE INFO

ABSTRACT

We present recent advances in phase-field crystal (PFC) modeling of crystal nucleation in simple undercooled liquids, where dynamics is based on hydrodynamic density relaxation, as opposed to the diffusive dynamics in colloid systems. Herein, we address two-step nucleation, the nucleation of new grains at the growth front, and crystal nucleation on the surface of foreign particles in flow. Owing to the different numerical complexity of these problems, we consider three different realizations of the hydrodynamic approach that are optimized to deal with the individual tasks. We show that during two-step nucleation taking place at high supersaturations, amorphous and layered two-dimensional quasicrystalline domains form simultaneously in the first stage, which is then followed by bcc nucleation/transformation of the existing solid into the stable body-centered structure. Next, the formation of satellite crystals at the solid-liquid interface, observed in molecular dynamics simulations are studied. We find that the interference of density waves ahead of the rough growth front may assist the formation of such satellite crystals. Finally, we show that, under appropriate conditions, fluid flow may tear off heterogeneously nucleated crystal particles from the surface of a curved substrate, as envisaged for colloidal systems.

1. Introduction

Crystal nucleation in highly non-equilibrium liquids is an essentially unsolved problem [1,2] in the sense that models that show some predictive force are usually based on molecular scale simulations relying on molecular dynamics (MD) and Monte Carlo techniques. While classical nucleation theory [2] that relies on cluster population dynamics of the Schmoluchowski type [2–6], captures qualitative features of the nucleation process, it also requires a number of assumptions. It is reasonable to expect that crystal nucleation (crystal formation on the nanoscale) and crystal growth taking place in the interfacial regime (also on the nanoscale) have common fundamentals. Accordingly, continuum models of the coarse grained type (e.g., phase field [7–13], PF; van der Waals [14], Cahn-Hilliard [15], and time dependent Ginzburg-Landau [16] theories) or those working on the molecular scale (various types of the classical density functional theory [17–27], DFT) successfully capture important features of nanoscale clusters, and proved useful in exploring nucleation and crystal growth in various systems. Indeed, the DFT models employed to crystal nucleation provided understanding reaching far beyond the classical nucleation theory [17–27]. Unfortunately, these models usually require a detailed knowledge of the system

investigated, and some assumptions due to the lack of input data. Therefore, matching to known model systems plays an important role in validating the assumptions used to make these models tractable [28].

Remarkably, even crystal growth in highly undercooled simple liquid is puzzling as a satisfactory agreement between MD simulations and theoretical predictions cannot be achieved [29,30]. Owing to the typically nanoscale dimensions of nuclei, which are comparable with the interface thickness, and the respective high curvature of the interface, additional complications occur in the case of nucleation. While these complications can be handled to some extent in the coarse grained continuum models, some other features are associated with the local molecular arrangement. For example, a rectangular inner corner is always a preferred nucleation site in the classical and coarse grained models [9], yet it is not so if the crystal has a triangular structure that is incompatible with the rectangular corner forcing thus the formation of a grain boundary [25].

Extensive microscopic information is available for crystal nucleation from two sources: (i) experiments on colloidal systems [1,31–39], and (ii) MD/Brownian dynamics (BD) simulations [1,40–49]. Experiments on colloids seem to indicate that crystal nucleation is a two-step process with an amorphous precursor, whose structural features determine the

---

structure of the forming crystal nucleus [36,37,39]. It has also been demonstrated by BD simulations that stresses building up in the curved crystal planes of heterogeneous nuclei on a spherical surface can peel off the nucleus, freeing the surface for further heterogeneous nucleation [47]. It is uncertain whether these complex phenomena do take place in simple liquids. Other open questions are the mechanism by which satellite nuclei form in the vicinity of growing crystallites [49], and the microscopic background of other mechanisms by which new orientations may appear at the growth front (Growth Front Nucleation, GFN) [50], phenomena that lead to the formation of such polycrystalline growth forms as spherulites, crystal sheaves, and disordered dendrites.

Recently, a broad range of molecular scale phenomena taking place in condensed matter transitions was investigated in the framework of a simplistic dynamical density functional theory, the phase-field crystal (PFC) model working on the diffusive timescale [51–53]. Attempts were made recently to combine the PFC approach with hydrodynamic density relaxation (HPFC) to attack transitions in simple liquids. Development of such models is not a trivial task, therefore, a variety of models based on different approximations have been put forward during the past years [54–60].

In this paper, we are going to use a HPFC approach for investigating the possibility of two-/multistep nucleation, heterogeneous nucleation in fluid flow, and GFN in highly undercooled simple liquids. Since we are interested in competing crystalline, amorphous, and liquid structures, we opt for HPFC approaches that do not rely on amplitude expansion. Therefore, for the present study, we have chosen a HPFC model we proposed some time ago [55,59] and its adaptations (e.g., [60]) to the problems specified above.

2. Hydrodynamic PFC models

2.1. PFC thermodynamics

In the PFC model, the local state of matter is characterized by a time-averaged particle density field, ρ. The dimensionless form of the free energy of the inhomogeneous liquid + crystal system taken relative to a homogeneous reference fluid (of density $\rho_{L,ref}$) can be given as.

$$\Delta F = \int d\mathbf{r} \left\{ \frac{\psi}{2} \left[-\varepsilon + \left(1 + \nabla^2\right)^2 \right] \psi + \frac{\psi^4}{4} \right\} \tag{1}$$

Here $\psi \propto (\rho - \rho_{L,ref})/\rho_{L,ref}$ is the scaled density difference, whereas ε is the reduced temperature that can be related to the bulk compressibility of the reference liquid, the bulk modulus of the solid and the density of the reference liquid. This form of the free energy functional can be deduced [52,53,61] from the perturbative classical density functional theory of Ramakrishnan and Yussouff [62]. Note that in 2D this free energy expression yields a phase diagram that consists of stability domains for the homogeneous (liquid), triangular crystal, and striped phases, whereas in 3D the phase diagram contains stability domains for the body centered cubic (bcc), face centered cubic (fcc), and hexagonal close packed (hcp) crystal structures, besides the homogeneous (liquid), triangular rod and lamellar phases (see e.g., [53]).

2.2. Hydrodynamic models of solidification

2.2.1. HPFC1:

This model [55] is based on *fluctuating nonlinear hydrodynamics* as formulated in [63,64]. The momentum transport and continuity equations were written in the form.

$$\frac{\partial \mathbf{p}}{\partial t} + \nabla \cdot (\mathbf{v} \otimes \mathbf{p}) = \nabla \cdot [\mathbf{R}(\rho) + \mathbf{D}(\mathbf{v}) + \mathbf{S}] \tag{2}$$

$$\frac{\partial \rho}{\partial t} + \nabla \cdot \mathbf{p} = 0 \tag{3}$$

Here $\mathbf{p}(\mathbf{r}, t)$ stands for the momentum, $\rho(\mathbf{r}, t)$ is the mass density, $\mathbf{v} = $

$\langle \mathbf{p} \rangle / \langle \rho \rangle$ the velocity, while $\nabla \cdot \mathbf{R} = -\rho \nabla \{\delta \Delta F[\rho]/\delta\rho\} \approx -\rho_0 \nabla \{\delta \Delta F[\rho]/\delta\rho\}$ the reversible stress tensor. $\delta \Delta F[\rho]/\delta\rho$ denotes the functional derivative of the free energy (shown in Eq. (1)) with respect to the particle density. ρ_0 denotes a reference density, $\mathbf{D} = \mu_S\{(\mathbf{v} \otimes \mathbf{p}) + (\mathbf{v} \otimes \mathbf{p})^T\} + [\mu_B - (2/3)\mu_S](\nabla \cdot \mathbf{v})$ is the dissipative stress tensor, whereas $\mathbf{S}$ is a stochastic momentum noise of correlation.

$$\langle S_{ij}(\mathbf{r}, t), S_{kl}(\mathbf{r}', t') \rangle = (2kT\mu_S) \times$$

$$\left[\left(\delta_{ik}\delta_{jl} - \delta_{jk}\delta_{il} \right) + \left(\frac{\mu_B}{\mu_S} - \frac{2}{3} \right) \delta_{ij}\delta_{kl} \right] \delta(\mathbf{r} - \mathbf{r}')\delta(t - t') \tag{4}$$

In this expression, μ_S and μ_B are the shear/bulk viscosities.

In computing the velocity in the hydrodynamic equations, we apply coarse-grained momentum and density fields: $\mathbf{v} = \langle \mathbf{p} \rangle / \langle \rho \rangle$. (For details see Ref. [55]). In a recent study, this approach indicated two possible mechanisms to form new orientations at the growth front [59]. In this work, we further explore these possibilities.

2.2.2. HPFC2:

A slightly different approximate formulation of the hydrodynamic PFC model was used in addressing heterogeneous nucleation on a curved surface in the presence of flow. The respective equations are as follows. Here $n = (\rho - \rho_{L,ref})/\rho_{L,ref}$, and.

$$\frac{\delta \Delta F}{\delta n} = V - \frac{an^2}{2} + \frac{bn^3}{3} + (1 - \widehat{c}_k)n \tag{5}$$

$$\phi_k = -\frac{(\nabla \cdot \mathbf{v})_k}{k^2}, \mathbf{u} = \mathbf{v} - \nabla\phi, \ \nabla \cdot \mathbf{u} = 0, \tag{6–8}$$

$$\frac{\partial \rho}{\partial t} = -\rho_0 \nabla \cdot \mathbf{v} - \nabla \cdot (\rho \mathbf{u}) \tag{9}$$

$$\frac{\partial \mathbf{v}}{\partial t} = -(\mathbf{u} \cdot \nabla)\mathbf{v} + \mu \Delta \mathbf{v} - \nabla \left(\frac{\delta \Delta F}{\delta \rho} + \zeta \right) - \nabla \cdot (\nabla \rho \otimes \nabla \rho) \tag{10}$$

Here μ is viscosity, ρ_0 is a constant density, V an external potential (defining the substrate), a and b are material parameters, $\widehat{c}_k$ is the Fourier transform of the two-particle direct correlation function, whereas $\mathbf{u}$ is the divergence-free part of velocity $\mathbf{v}$ used in the advection of mass density. ϕ_k is a scalar field, while ζ a noise term. Finally, the term $\nabla \cdot (\nabla \rho \otimes \nabla \rho)$ is associated with the Korteweg stress tensor. Note that Eq. (5) relies on a form of the free energy expressed in terms of n (see Eqs. (12) and (13) in [55]), which is equivalent to Eq. (1), however, supplemented here with a potential energy term for the substrate.

2.2.3. sHPFC:

The numerical solution of models HPFC1 and HPFC2 is computationally demanding in 3D, therefore, a simplified HPFC approach was proposed [60] that relies on linearized hydrodynamics. Along this line, we first postulate that the velocity and density gradients are small, and the advection term is negligible, then we insert the time derivative of the continuity equation into the divergence of the momentum transport equation. This yields a specific form of the DDFT/HI model derived by Kikkinides and Monson, an approach that was used successfully for describing nanoscale capillary waves [65]:

$$\frac{\partial^2 \rho}{\partial t^2} + \alpha \frac{\partial \rho}{\partial t} = \Delta \left\{ \frac{\delta \Delta F}{\delta \rho} + \beta \frac{\partial \rho}{\partial t} \right\} + \nabla \cdot \nabla \cdot \mathbf{S} \tag{11}$$

In this expression, α and $\beta = \{(4/3)\mu_S + \mu_B\}/\rho$ are damping coefficients, and $\delta \Delta F[\rho]/\delta\rho$ is the functional derivative of the free energy (shown in Eq. (1)) with respect to the density field, whereas $\mathbf{S}$ is the same stochastic momentum tensor that was used in Eq. (4). Assuming $\beta = 0$, and omitting the noise term, one recovers the modified PFC (MPFC) model proposed in [66,67]. Much like the full HPFC model, at small undercoolings the sHPFC approach recovers a steady state growth velocity $v \propto 1/\mu_S$, and longitudinal and transversal quasi-phonons of
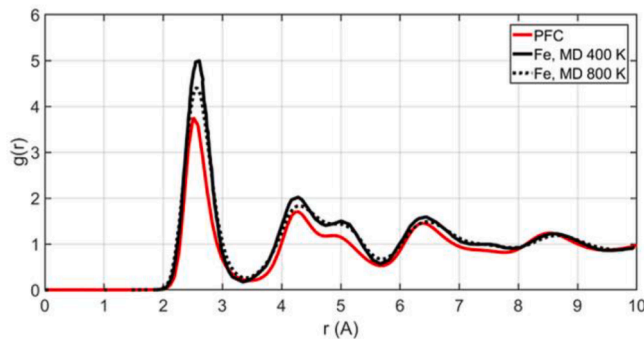
Fig. 1. Pair distribution function g(r) for amorphous iron as predicted by the PFC model [13], and MD simulations [73].

proper dispersion in the crystal. Herein, we use two forms of the linearized HPFC approach (MPFC: $\alpha = 1$ and $\beta = 0$, and sHPFC: $\alpha = 0$ and $\beta = 1$) to extend a previous study [60] that addressed the structural aspects of crystal nucleation in 3D simple liquids.

2.3. PFC with diffusive dynamics

In the majority of PFC models, diffusive density relaxation was assumed [21–23,25,51–53,61], which is therefore termed diffusive PFC model (DPFC). This type of dynamics is realized by the following dimensionless equation of motion:

$$\frac{\partial \psi}{\partial t} = \nabla \cdot \left\{ \nabla \frac{\delta \Delta F}{\delta \psi} \right\} + \zeta. \tag{12}$$

A colored Gaussian flux noise ζ of correlation $\langle \zeta(\mathbf{r},t)\zeta(\mathbf{r'},t') \rangle = \xi^2 \nabla^2 g(|\mathbf{r} - \mathbf{r'}|, \sigma)\delta(t - t')$ is incorporated into the governing equation to represent the density fluctuations. Here ξ is the noise strength, and a high frequency cutoff is realized by the function $g(|\mathbf{r} - \mathbf{r'}|, \sigma)$ [22,23] that removes the wavelengths shorter than the atomic spacing (σ). At small driving forces for crystallization: (i) at small undercoolings or supersaturations growth is diffusion controlled and $v \propto t^{-1/2}$, whereas (ii) at large driving forces, where diffusion length $l_D = D/v$ becomes comparable to the interface thickness a transition is observed to a diffusionless fast growth mode displaying steady state growth ($v = $ const.), as expected for colloids .

2.4. Numerical methods

The governing equations of models HPFC1, HPFC2, MPFC, and sHPFC were solved in dimensionless form, relying on a pseudospectral spatial scheme [68] combined with either semi-implicit time stepping (DPFC), forward Euler time stepping (HPFC2), or a second-order Runge-Kutta time stepping (HPFC1, MPFC, and sHPFC), respectively. Uniform rectangular grids were used in both 2D and 3D, while employing periodic boundary conditions on all sides, unless stated otherwise. The computations were performed on high-end Graphics Processing Units.

2.5. Materials/model parameters used in the simulations

The single-mode PFC model can be fitted to iron [69,70], yielding fairly realistic properties for the interfacial free energy and its anisotropy, the solid/liquid bulk moduli, though the expansion on melting is somewhat overestimated (see dataset GL-PFC in Table I of Ref [70]). In the HPFC1 and HPFC2 models, the physical properties of iron were used as specified in Refs. [55,59,70]. Here, the relative free energy ΔF (Eqs. (12) and (13) of [55]) was computed after approximating the Fourier transform of the direct correlation function as $\widehat{C}_k = C_0 + C_2 k^2 + C_4 k^4$, where $C_0 = -10.9153$, $C_2 = 2.6$ Å^2, $C_4 = -0.1459$ Å^4, $a = 0.6917$ and $b = 0.08540$ are data for iron taken from [70]. The corresponding melting point properties are $\psi_L = -0.1982$ and $\varepsilon_L = 0.0923$, whereas the respective critical properties are $\psi_c = -0.1754$ and $\varepsilon_c = 0.1178$. We note that this free energy expression can be transformed into Eq. (1) via straightforward manipulations [53]. Accordingly, Eq. (5) follows from the same free energy, however, with a potential energy term added. The dimensionless time and spatial steps used here were $\Delta t = 0.025$ and $\Delta x = 1.001 \times (4\pi/\sqrt{3})/8 \approx 0.9078$.

In 3D simulations based on the DPFC, MPFC, and sHPFC models, parameter values taken from [60] were used in Eq. (1). A scaled density of $\psi_0 = -0.2720$ was chosen, whereas different reduced temperatures falling between the liquidus $\varepsilon_L = 0.1548$ and the linear stability limit $\varepsilon_c = 0.2220$ were used. If not stated otherwise, the DPFC, MPFC, and sHPFC simulations were performed at a scaled density of $\psi_0 = -0.272$, and reduced temperature $\varepsilon = 0.2$. A noise strength of $\xi = 0.005$ was used in all three models. In these simulations the dimensionless time and spatial steps were $\Delta t = 0.01$ and $\Delta x = 1.0$.

Instantaneous quenching with these model parameters yields an amorphous state of reasonable structural properties [22,71–73] (Fig. 1).

In all cases, when transforming the simulation results to dimensional form, the viscosity (HPFC1, HPFC2, MPFC, and sHPFC) or the self-
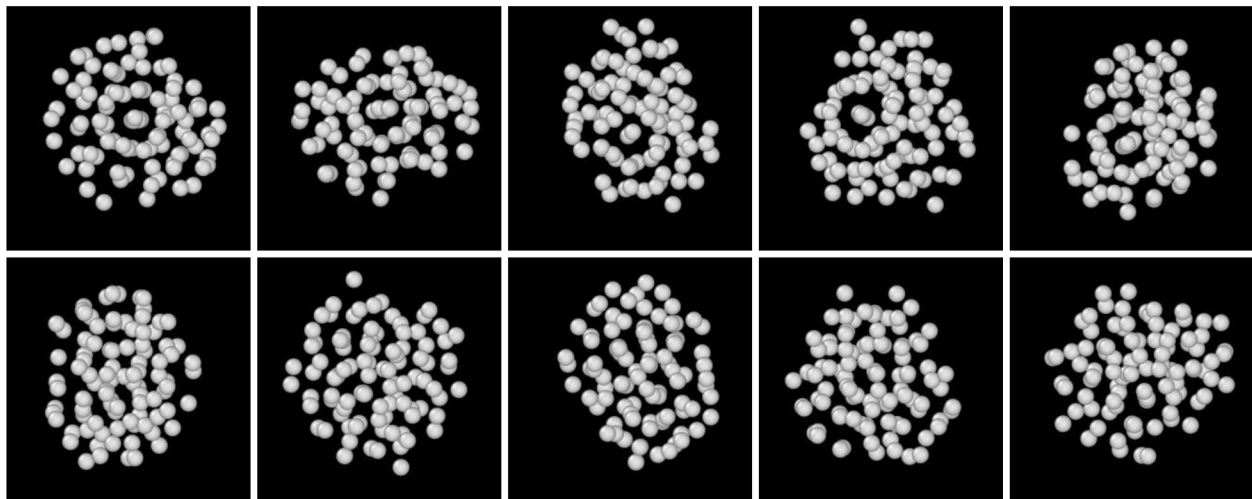

Fig. 2. Different views of the early stage cluster from an sHPFC simulation (reproduced from [60] under Creative Commons Attribution (CC BY) license). Note that the views in the upper row show some degree of order, structural order in the bottom row is less obvious. A fraction of a 512^3 simulation (corresponding to about 3.6×10^5 atoms) is shown.
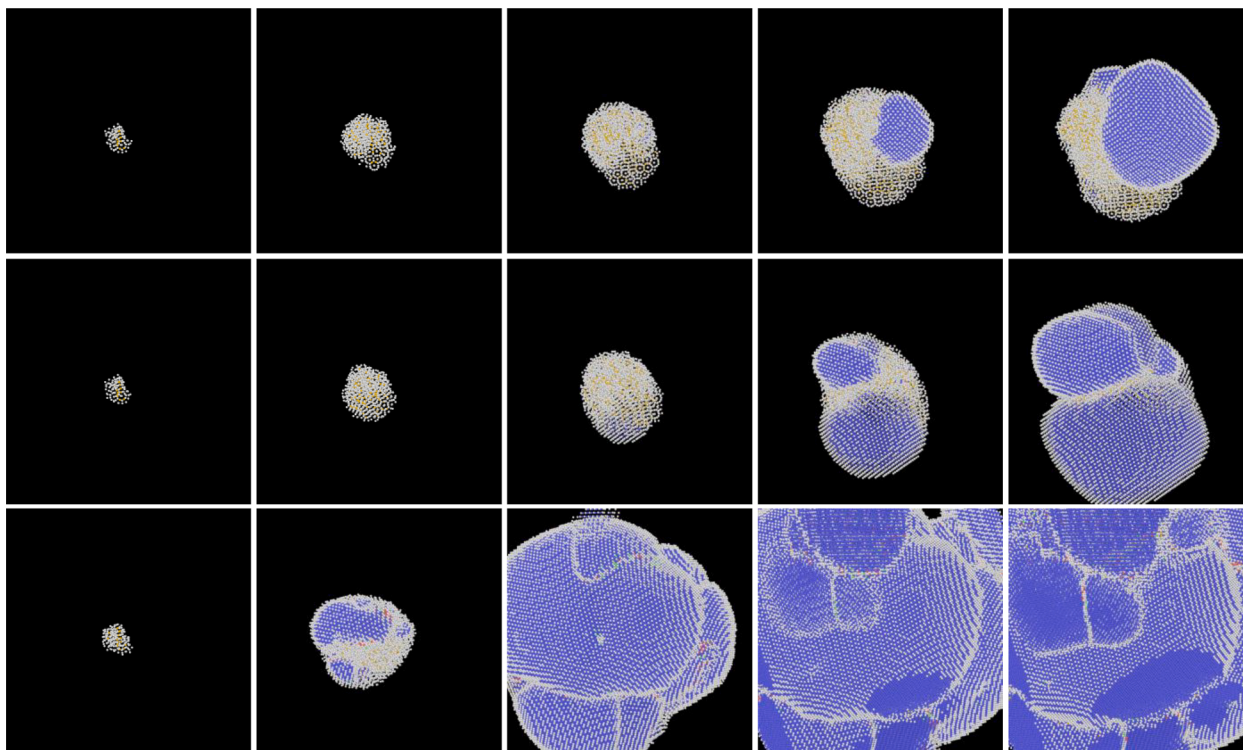
Fig. 3. Time evolution of the same early stage cluster within the DPFC (1st row), MPFC (2nd row), and sHPFC (3rd row) models at reduced times $t = 1500, 3000,$ 4500, 6000, and 7500. A view is shown, from which the presence of a layered 2D QC structure is evident. Polyhedral template matching was used to color the atoms according to their neighborhood: yellow – icosahedral; blue – bcc; red – hcp; white - unidentified. The solid–liquid surface is covered by atoms of unidentified neighborhood, as they have less neighbors. Snapshots of 512^3 simulations corresponding to about 3.6×10^5 atoms are shown. The average growth rate of the DPFC and MPFC results are fairly close to each other as reported in [60], whereas the growth of the bcc phase in the sHPFC model is considerably faster. (For interpretation of the references to color in this figure legend, the reader is referred to the web version of this article.)
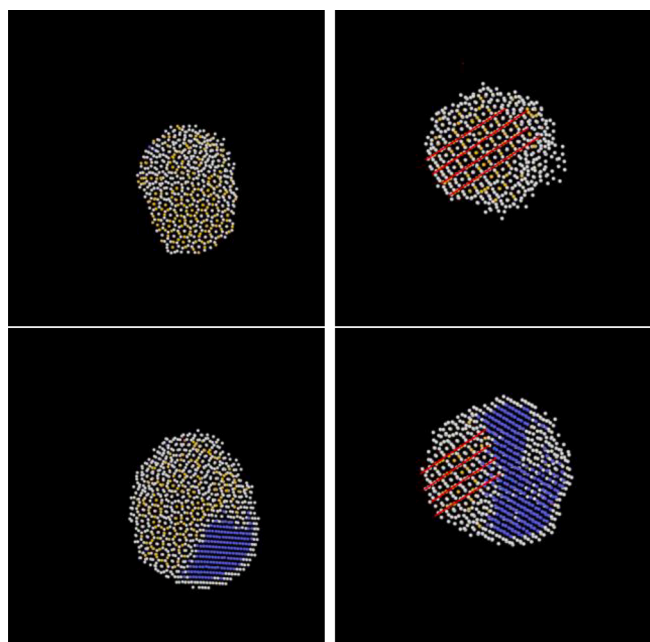

Fig. 4. Layered 2D QC-like structures in the DPFC (upper row) and MPFC (lower row) clusters. The top view (left) and a side view (right) are shown at dimensionless time $t = 5000$. Six molecular layers' thick slices are displayed. The red lines on the right indicate the side view the 2D QC-like planes. Coloring is the same as in Fig. 3. (For interpretation of the references to color in this figure legend, the reader is referred to the web version of this article.)

diffusion coefficient (DPFC) sets the physical time scale of the crystallization process.

2.6. Structural analysis

The average bond order parameters $\overline{q}_l^k$ of Lechner and Dellago [74] were used to analyze the structural aspects of the solid domains. These order parameters incorporate structural information from the 1st and 2nd neighbor shells:

$$\overline{q}_l^k = \left\{ \frac{4\pi}{2l+1} \sum_{m=-l}^{l} \left| \overline{q}_{lm}^k \right|^2 \right\}^{1/2}, \text{ where } \overline{q}_{lm}^k = \frac{1}{N_b^k + 1} \sum_{i=0}^{N_b^k} q_{lm}^i \text{ and } q_{lm}^i$$

$$= \frac{1}{n_b^i} \sum_{j=1}^{n_b^i} Y_{lm}(\mathbf{r}_{ij})$$

$$(13\text{–}15)$$

In these expressions, N_b^k is the number of neighbors of the kth particle, n_b^i are the number of the first neighbors of the ith neighbor of particle k. Y_{lm} denotes the spherical harmonics of degree l and order m, whereas $\mathbf{r}_{ij}$ is the vector between the ith first neighbor atom and its jth first neighbor. The $\overline{q}_4 - \overline{q}_6$ map is widely used to distinguish the bulk bcc, hcp, fcc and liquid structures from molecular dynamics simulations [1,22,29,40–42,45] and colloid experiments [32,37]. They were used successfully to visualize structural transitions during crystallization processes.

In addition to this, we applied the Polyhedral Template Matching (PTM) [75] method implemented in OVITO [76] for analyzing the local structure.

In the case of the 2D HPFC1 simulations, we used Voronoi polyhedral (polygonal) analysis, and a "hexatic" bond order parameter $g_6 =$
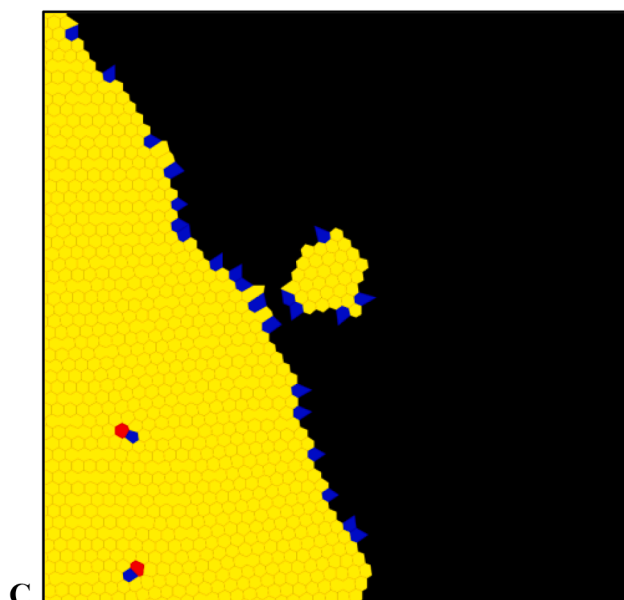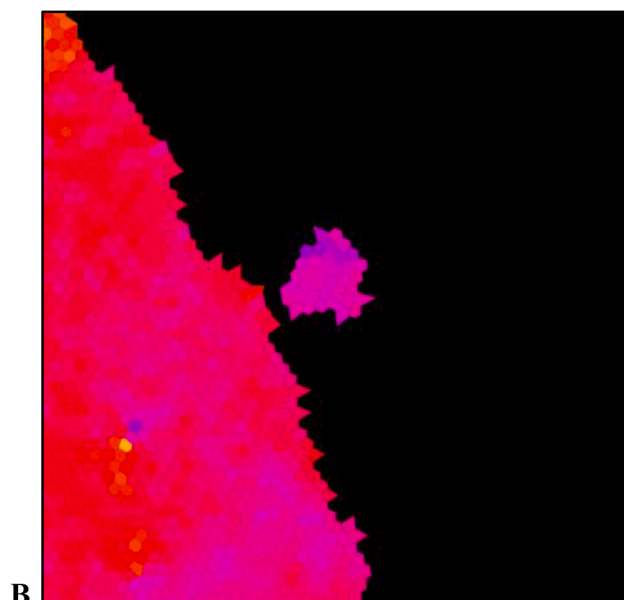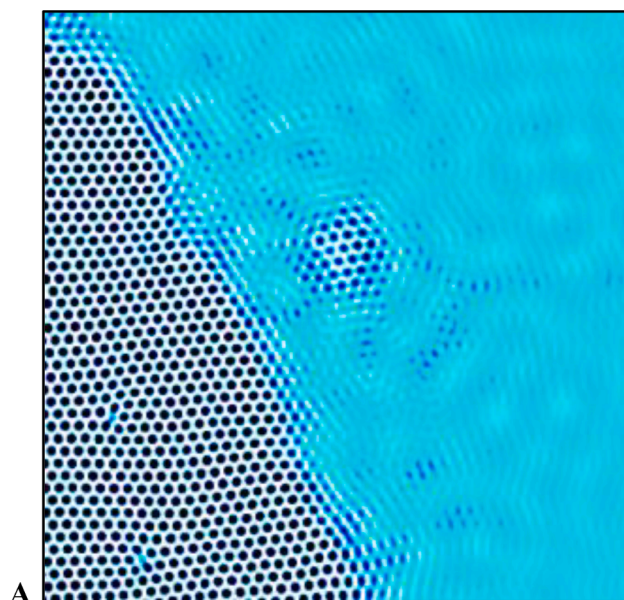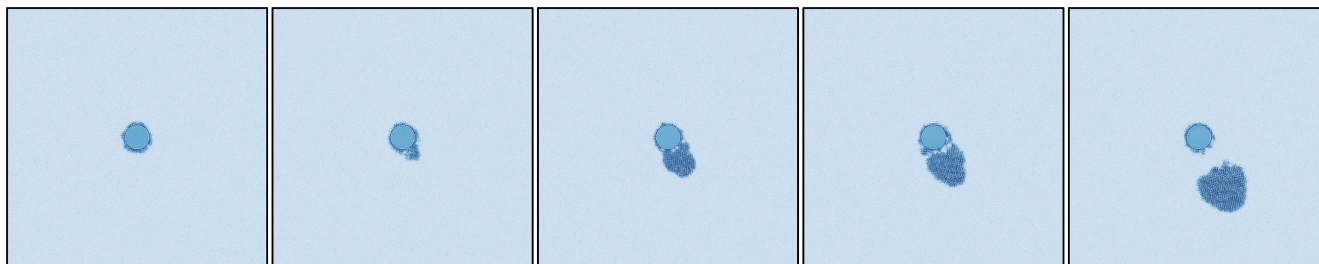
(caption on next page)

Fig. 6. Snapshots made at reduced times $t = 300, 1600, 3000, 3500$, and 4000 of simulation performed using the HPFC2 model that show heterogeneous crystal nucleation on the surface of a circular foreign particle and flow-induced removal of the nucleated crystal.

$\sum_j \exp(-6i\theta_j)$ to visualize crystal grains (crystallographic orientation) and crystal defects. Here θ_j is the angle to the jth neighbor in the laboratory frame. The phase of g_6 represents the local crystallographic orientation.

3. Results and discussion

3.1. Structural aspects of nucleation and early stage growth

In a previous work [60], we investigated structural changes during the early stage of crystal formation within the linearized HPFC and DPFC models. We found that the first appearing solid structure appears to be partly ordered, as concentric somewhat distorted ring-like atomic arrangements were seen from certain directions (Fig. 2). In this early stage clusters, a higher number of atoms with icosahedral neighborhood has been seen than in the Lennard-Jones (LJ) fluid. On the basis of their position on the $\overline{q}_4 - \overline{q}_6$ bond order parameter map, or the $\overline{q}_6$-based color scheme by Kawasaki and Tanaka [45] these early stage structures cannot be distinguished from the liquid structure of the LJ system.

Herein, we specify further the structural evolution of these early stage solid molecular arrangements. We have taken a state that contains such a cluster in the DPFC model, obtained using the parameter values defined in subsection 2.5. This state was then used as an initial condition for simulations performed at $\varepsilon = 0.175$ within the DPFC, MPFC, and sHPFC models, keeping the other conditions unchanged. The time evolution of the respective clusters is viewed in Fig. 3 from the same direction: In all cases three obvious domains appear: amorphous, a 2D quasicrystal-like (QC), and bcc. During the early stage only the first two is present, later the bcc phase appears by heterogeneous nucleation and suppress them in the long run. In accord with earlier results [60], in the overall growth rate of the DPFC and MPFC models clusters are similar, whereas the transformation to bcc and its growth rate are faster in the sHPFC model. We have used the PTM method to identify the neighborhoods of the respective atoms. While with the applied PTM settings, the bcc structure was reliably identified, we could not identify the local structure in the "amorphous" domain, whereas in the QC-like structure a large fraction of the atoms qualified as of icosahedral neighborhood.

The Kawasaki-Tanaka type coloring based on $\overline{q}_6$ distinguished three structures (amorphous, medium range crystal-like order – MRCO, and bcc) in similar clusters [60], however, the $g(r)$ of the amorphous and MRCO structures fall quite close [60], therefore, the latter may be regarded a kind of transition layer between the amorphous and bcc structures. In contrast, it is easy to distinguish the QC-like structure from the view shown in Fig. 3 even by the naked eye.

Next, we concentrate on this newly found structure. Views showing the quasi 2D QC molecular planes and a perpendicular direction are presented in Fig. 4 on the left and right, respectively. Within the quasi 2D QC molecular planes, a network of 10 and 12 membered rings are seen, which are built dominantly of atoms of icosahedral neighborhood. In the perpendicular direction, a molecular arrangement of square-lattice-type symmetry is found, with lower density of molecules of icosahedral neighborhood. These results are consistent with a layered 2D quasi-crystalline structure that is periodic in one direction.

We note that 2D and 3D QC structures were studied extensively within two- and higher mode PFC models that rely on two or more specific wavelengths [77–85]. To our understanding, the present work is the first, which indicates that nucleation of a layered 2D QC structure (a type discussed in [85,86]) is possible in the single-mode PFC model. We note, furthermore, that nucleation and growth of icosahedral clusters of unordered shape were reported in MD simulations using a Dzugutov type potential (of a minimum at r_0 and a maximum at about $r_0\sqrt{2}$) [87,88], which was developed to realize a monatomic glass former. A similar effective pair potential was evaluated for the single mode PFC model [22]. However, in [88] the icosahedral structure has a tetra-
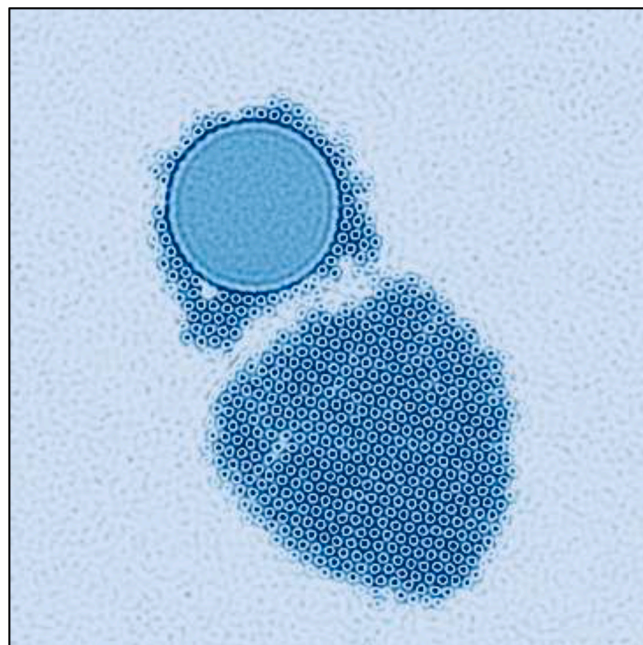

Fig. 7. Separation of the crystal covered circular substrate and crystallite escaping the substrate at reduced time $t = 3700$.

helical atomic arrangement, which does not appear to be the case in our simulations. Finally, experiments on specific metal alloy melts indicate icosahedral-QC-enhanced nucleation of the fcc phase [89].

3.2. Formation of satellite crystals in the HPFC1 model

In recent extremely large scale MD simulations for undercooled molten iron [49], it has been reported that "satellite" nuclei form in the vicinity of already existing crystals, i.e., the probability of forming nuclei appears to be higher near the growth front than in the bulk liquid. The authors noted furthermore that in this domain, the probability of atoms of icosahedral neighborhoods is higher than in the bulk liquid and associated the formation of satellite nuclei with this finding [49].

A similar phenomenon, i.e., enhanced nucleation close to the growth front has been reported within a HPFC1 model with parameters of iron at extreme supersaturations [59]. In these simulations, crystallization was initiated by a potential template leading to the formation of a triangular neighborhood of 7 atoms at the natural interatomic distance of the stable triangular crystal. After a very short transient time, which is far shorter than the incubation time of homogeneous crystal nucleation, a roughly triangular crystal seed formed (or in the absence of noise a perfect hexagonal crystal), which attained an increasingly irregular shape as it grew. Well before homogeneous nucleation set in, small nuclei formed exclusively in the vicinity of the growth front, creating orientations that may deviate considerably from the growing crystal. The formation of these "satellite" crystals can be attributed to the interference of density waves that extend into the undercooled liquid state and originate from sections of a rough crystal-liquid interface, which may occasionally create a template (density pattern) that helps crystal nucleation. This is indeed a phenomenon that can exist only in the close vicinity of the crystal-liquid interface (see Fig. 5), and may be viewed as a possible microscopic mechanism for GFN.

3.3. Heterogeneous nucleation in flow in the HPFC2 model

One of the main improvements this model realizes is that owing to the presence of pure advection due to the divergence-free velocity **u** in the kinetic equation enables synchronous motion and rotation of the crystal structure together with the solid cluster. To demonstrate its capabilities, we attempted to reproduce a prediction made via Brownian dynamics simulation for colloidal liquids [47], i.e., that due the stress building up crystallites nucleated heterogeneously on a curved surface (substrate), beyond a critical size the crystal peels off the substrate and may be carried away by flow enabling repetitive nucleation by a single nucleation center. In order to approximate this situation, we introduced a circular substrate defined by adding an appropriate potential energy term, $V(\mathbf{r})\psi$, to the free energy density. Boundary conditions prescribing motion from left to right (of velocity v_0) were prescribed at the upper and bottom edges of the simulation box whereas downward motion of the same velocity was assigned to the vertical edges. We note that with the exception of this section, forced flow is not prescribed in the present simulations (e.g., in sections 3.1 and 3.2 only density change upon solidification may cause flow). Snapshots displaying the simulation results are presented in Figs. 6 and 7. The crystalline phase nucleates with curved crystal planes, and when it grows large enough, the flow cracks the crystal along its faults, and carries it away from the substrate. The present 2D model contains the main ingredients (flow, nucleation and growth, elasticity, and plasticity) needed to describe such a phenomenon, and may thus serve as a basis for developing a more quantitative approach.

4. Summary

We have addressed three topics using simple classical density functional approaches relying on different (application oriented) realizations of hydrodynamic density relaxation in two- and three dimensions, while taking the free energy functional from the single-mode Phase-Field Crystal model. We have shown the following:

(1) In *single-mode* PFC models relying on diffusive dynamics (DPFC) and linearized hydrodynamics (MPFC and SHPFC) we found that at the early stage of solid cluster formation two structures occur: an amorphous one, and a layered 2D quasicrystal-like (QC) structure that is periodic in the third dimension. The stable bcc phase nucleates on these structures in a heterogeneous manner, and grows faster, and devours them as time elapses. The transformation to bcc structure is the fastest in the case of sHPFC dynamics.

(2) Within the HPFC1 model (that relies on coarse grained momentum and density fields in computing the velocity in the hydrodynamic equations), we searched for a possible analogue of satellite crystal formation in the vicinity of the growth front, a phenomenon discovered in extreme large molecular dynamics simulation. It appears that interference of density waves forming part of the diffuse interface of uneven shape may occasionally create templates that assist crystal nucleation, even if bulk homogeneous nucleation is not yet active.

(3) Using the HPFC2 model, we investigated heterogeneous nucleation on a curved surface (circular substrate) in the presence of fluid flow. Under appropriate conditions, after growing large enough the nucleated crystal separates from the substrate as an interaction of packing defects and the force exerted by the flow on the nucleated crystal.

Work is underway to clarify further these issues, especially why/how the layered 2D QC-like structure forms in the single-mode theory, and how this phenomenon depends on the interaction potential.

CRediT authorship contribution statement

Frigyes Podmaniczky: Investigation, Formal analysis, Software, Validation, Visualization, Writing – review & editing. **László Gránásy:** Conceptualization, Investigation, Writing – original draft, Writing – review & editing, Funding acquisition

Declaration of Competing Interest

The authors declare that they have no known competing financial interests or personal relationships that could have appeared to influence the work reported in this paper.

Acknowledgments

References

[1] H. Tanaka, Roles of Bond Orientational Ordering in Glass Transition and Crystallization, J. Phys.: Condens. Matter 2011 (23) (2011), 284115, https://doi.org/10.1088/0953-8984/23/28/284115.

[2] K.F. Kelton, A.L. Greer, Nucleation in Condensed Matter: Applications in Materials Science and Biology, Elsevier, Amsterdam, 2010.

[3] K.F. Kelton, Crystal Nucleation in Liquids and Glasses, Solid State Phys. 45 (1991) 75, https://doi.org/10.1016/S0081-1947(08)60144-7.

[4] J.D. Gunton, M. San Miguel, P.S. Sahni, The dynamics of first order phase transitions, in: C. Domb, J. Lebowitz (Eds.), Phase Transitions and Critical Phenomena, 1st ed., Academic Press, London, 1983, pp. 267–466.

[5] J.K.G. Dhont, An Introduction to Dynamics of Colloids, 1st ed., Elsevier, Amsterdam, 1996.

[6] H. Risken, The Fokker-Planck Equation: Methods of Solution and Applications, 3rd ed., Springer, Berlin, 1996.

[7] A. Roy, J. Rickman, J. Gunton, K. Elder, Simulation study of nucleation in a phase-field model with nonlocal interactions, Phys. Rev. E 57 (3) (1998) 2610–2617, https://doi.org/10.1103/PhysRevE.57.2610.

[8] L. Gránásy, T. Börzsönyi, T. Pusztai, Nucleation and bulk crystallization in binary phase field theory, Phys. Rev. Lett. 88 (2002), 206105, https://doi.org/10.1103/PhysRevLett.88.206105.

[9] M. Castro, Phase-field approach to heterogeneous nucleation, Phys. Rev. B 67 (2003), 035412, https://doi.org/10.1103/PhysRevB.67.035412.

[10] L. Gránásy, T. Pusztai, D. Saylor, J.A. Warren, Phase field theory of heterogeneous crystal nucleation, Phys. Rev. Lett. 98 (2007), 035703, https://doi.org/10.1103/PhysRevLett.98.035703.

[11] J.A. Warren, T. Pusztai, L. Környei, L. Gránásy, Phase field approach to heterogeneous crystal nucleation in alloys, Phys. Rev. B. 79 (2009), 014204, https://doi.org/10.1103/PhysRevB.79.014204.

[12] H. Emmerich, P. Virnau, G. Wilde, R. Spatschek, Heterogeneous nucleation and microstructure formation: Steps towards a system and scale bridging understanding, Eur. Phys. J. Spec. Top. 223 (3) (2014) 337–346, https://doi.org/10.1140/epjst/e2014-02094-1.

[13] L. Gránásy, G.I. Tóth, J.A. Warren, F. Podmaniczky, G. Tegze, L. Rátkai, T. Pusztai, Phase-field modeling of crystal nucleation in undercooled liquids – A review, Prog. Mater. Sci. 106 (2019), 100569, https://doi.org/10.1016/j.pmatsci.2019.05.002.

[14] J.D. van der Waals, Thermodinamische Theorie der Capillarri-teit. Koninklijke Akademie van Wettenschappen te Amsterdam, Erste Sectie, Deel 1, No. 8. (Johannes Müller, Amsterdam, 1893), pp. 1–56.

[15] J.W. Cahn, J.E. Hilliard, Free energy of a nonuniform system. III. Nucleation in a two-component incompressible fluid, J. Chem. Phys. 31 (3) (1959) 688–699, https://doi.org/10.1063/1.1730447.

[16] K. Binder, Time-dependent Ginzburg-Landau theory of nonequilibrium relaxation, Phys. Rev. B 8 8 (7) (1973) 3423–3438, https://doi.org/10.1103/PhysRevB.8.3423.

[17] P. Harrowell, D.W. Oxtoby, A molecular theory of crystal nucleation from the melt, J. Chem. Phys. 80 (4) (1984) 1639–1646, https://doi.org/10.1063/1.446864.

[18] L.V. Mikheev, A.A. Chernov, Mobility of a diffuse simple crystal melt interface, J. Cryst. Growth 112 (2–3) (1991) 591–596, https://doi.org/10.1016/0022-0248(91)90340-B.

[19] Y.C. Shen, D.W. Oxtoby, bcc symmetry in the crystal-melt interface of Lennard-Jones fluids examined through density functional theory, Phys. Rev. Lett. 77 (17) (1996) 3585–3588, https://doi.org/10.1103/PhysRevLett.77.3585.

[20] Y.C. Shen, D.W. Oxtoby, Nucleation of Lennard-Jones fluids: A density functional approach, J. Chem. Phys. 105 (15) (1996) 6517–6524, https://doi.org/10.1063/1.472461.

[21] R. Backofen, A. Voigt, A phase-field-crystal approach to critical nuclei, J. Phys.: Condens. Matter 22 (36) (2010), 364104, https://doi.org/10.1088/0953-8984/22/36/364104.

[22] G.I. Tóth, T. Pusztai, G. Tegze, G. Tóth, L. Gránásy, Amorphous nucleation precursor in highly nonequilibrium fluids, Phys. Rev. Lett. 107 (2011), 175702, https://doi.org/10.1103/PhysRevLett.107.175702.

[23] G.I. Tóth, G. Tegze, T. Pusztai, L. Gránásy, Heterogeneous crystal nucleation: The effect of lattice mismatch, Phys. Rev. Lett. 108 (2012), 025502, https://doi.org/10.1103/PhysRevLett.108.025502.

[24] T. Neuhaus, A. Hartel, M. Marechal, M. Scmiedeberg, H. Löwen, Density functional theory of heterogeneous crystal nucleation, Eur. Phys. J. Spec. Topics 228 (2014) 373, https://doi.org/10.1140/epjst/e2014-02097-x.

[25] L. Gránásy, F. Podmaniczky, G.I. Tóth, G. Tegze, T. Pusztai, Heterogeneous nucleation of/on nanoparticles: a density functional study using the phase-field crystal model, Chem. Soc. Rev. 43 (2014) 2159, https://doi.org/10.1039/C3CS60225G.

[26] J.F. Lutsko, J. Lam, Classical density functional theory, unconstrained crystallization, and polymorphic behavior, Phys. Rev. E 98 (2018), 012604, https://doi.org/10.1103/PhysRevE.98.012604.

[27] J.F. Lutsko, How crystals form: a theory of nucleation pathways, Sci. Adv. 5 (2019) eaav7399, https://doi.org/10.1126/sciadv.aav7399.

[28] J.J. Hoyt, M. Asta, A. Karma, Atomistic and continuum modeling of dendritic solidification, Mater. Sci. Eng. R 41 (2003) 121, https://doi.org/10.1016/S0927-796X(03)00036-6.

[29] G. Sun, J. Xu, P. Harrowell, The mechanism of the ultrafast crystal growth of pure metals from their melts, Nature Mater. 17 (10) (2018) 881–886, https://doi.org/10.1038/s41563-018-0174-6.

[30] Q. Gao, J. Ai, S. Tang, M. Li, Y. Chen, J. Huang, H. Tong, L. Xu, L. Xu, H. Tanaka, P. Tan, Fast crystal growth at ultra-low temperatures, Nature Mater. 20 (10) (2021) 1431–1439, https://doi.org/10.1038/s41563-021-00993-6.

[31] O. Galkin, P. Vekilov, Proc. Natl. Acad. Sci. U. S. A. 97 (2000) 6277, https://doi.org/10.1073/pnas.110000497.

[32] U. Gasser, E.R. Weeks, A. Schofield, P.N. Pusey, D.A. Weitz, Real-Space Imaging of Nucleation and Growth in Colloidal Crystallization, Science 292 (2001) 258, https://doi.org/10.1126/science.1058457.

[33] A. Yethiraj, Tunable Colloids: Control of Colloidal Phase Transitions with Tunable Interactions, Soft Matter 3 (2007) 1099, https://doi.org/10.1039/B704251P.

[34] V. Prasad, D. Semwogerere, E.R. Weeks, Confocal microscopy of colloids, J. Phys. Condens. Matter 19 (11) (2007), 113102, https://doi.org/10.1088/0953-8984/19/11/113102.

[35] H.J. Schöpe, G. Bryant, W. van Megen, Two-Step Crystallization Kinetics in Colloidal Hard-Sphere Systems, Phys. Rev. Lett. 96 (2006), 175701, https://doi.org/10.1103/PhysRevLett.96.175701.

[36] T.H. Zhang, X.Y. Liu, How does a transient amorphous precursor template crystallization, J. Am. Chem. Soc. 129 (44) (2007) 13520–13526, https://doi.org/10.1021/ja073598k.

[37] P. Tan, N. Xu, L. Xu, Visualizing kinetic pathways of homogeneous nucleation in colloidal crystallization, Nat. Phys. 10 (2014) 73–79, https://doi.org/10.1038/nphys2817.

[38] Y.i. Peng, F. Wang, Z. Wang, A.M. Alsayed, Z. Zhang, A.G. Yodh, Y. Han, Two-step nucleation mechanism in solid-solid phase transitions, Nat. Mater. 14 (1) (2015) 101–108, https://doi.org/10.1038/nmat4083.

[39] F. Zhang, Nonclassical nucleation pathways in protein crystallization, J. Phys. Condens. Matter 29 (44) (2017), 443002, https://doi.org/10.1088/1361-648X/aa8253.

[40] P.R. ten Wolde, M.J. Ruiz-Montero, D. Frenkel, Numerical Evidence for bcc Ordering at the Surface of a Critical fcc Nucleus, Phys. Rev. Lett. 75 (1995) 2714, https://doi.org/10.1103/PhysRevLett.75.2714.

[41] S. Auer, D. Frenkel, Prediction of absolute crystal-nucleation rate in hard-sphere colloids, Nature 409 (6823) (2001) 1020–1023, https://doi.org/10.1038/35059035.

[42] S. Auer, D. Frenkel, Numerical prediction of absolute crystallization rates in hard-sphere colloids, J. Chem. Phys. 120 (6) (2004) 3015–3029, https://doi.org/10.1063/1.1638740.

[43] R.S. Aga, J.R. Morris, J.J. Hoyt, M. Mendelev, Quantitative parameter-free prediction of simulated crystal-nucleation times, Phys. Rev. Lett. 96 (2006), 245701, https://doi.org/10.1103/PhysRevLett.96.245701.

[44] T. Schilling, H.J. Schöpe, M. Oettel, G. Opletal, I. Snook, Phys. Rev. Lett. 105 (2010), 025701, https://doi.org/10.1103/PhysRevLett.105.025701.

[45] T. Kawasaki, H. Tanaka, Formation of a crystal nucleus from Liquid, Proc. Nat. Acad. Sci. USA 107 (32) (2010) 14036–14041, https://doi.org/10.1073/pnas.1001040107.

[46] L. Filion, R. Ni, D. Frenkel, M. Dijkstra, Simulation of nucleation in almost hard-sphere colloids: The discrepancy between experiment and simulation persists, J. Chem. Phys. 134 (13) (2011), 134901, https://doi.org/10.1063/1.3572059.

[47] E. Allhyarov, K. Sandomirski, S.U. Egelhaaf, H. Löwen, Crystallization seeds favour crystallization only during initial growth, Nature Commun. 6 (2015) 7110, https://doi.org/10.1038/ncomms8110.

[48] Y. Shibuta, K. Oguchi, T. Takaki, M. Ohno, Homogeneous nucleation and microstructure evolution in million-atom molecular dynamics simulation, Sci. Rep. 5 (2015) 13534, https://doi.org/10.1038/srep13534.

[49] Y. Shibuta, S. Sakane, E. Miyoshi, S. Okita, T. Takaki, M. Ohno, Heterogeneity in homogeneous nucleation from billion-atom molecular dynamics simulation of solidification of pure metal, Nature Commun. 8 (2017) 10, https://doi.org/10.1038/s41467-017-00017-5.

[50] L. Gránásy, L. Rátkai, A. Szállás, B. Korbuly, G.I. Tóth, L. Környei, T. Pusztai, Phase-field modeling of polycrystalline solidification: From needle crystals to spherulites — A review, Metall. Mater. Trans. A 45 (2014) 1694–1719, https://doi.org/10.1007/s11661-013-1988-0.

[51] K.R. Elder, M. Katakowski, M. Haataja, M. Grant, Modeling Elasticity in Crystal Growth, Phys. Rev. Lett. 88 (2002), 245701, https://doi.org/10.1103/PhysRevLett.88.245701.

[52] K.R. Elder, N. Provatas, J. Berry, P. Stefanovic, M. Grant, Phase-Field Crystal Modeling and Classical Density Functional Theory of Freezing, Phys. Rev. B 75 (2007), 064107, https://doi.org/10.1103/PhysRevB.75.064107.

[53] H. Emmerich, H. Löwen, R. Wittkowski, T. Gruhn, G.I. Tóth, G. Tegze, L. Gránásy, Phase-Field-Crystal Models for Condensed Matter Dynamics on Atomic Length and Diffusive Time Scales: An Overview, Adv. Phys. 61 (2012) 665, https://doi.org/10.1080/00018732.2012.737555.

[54] A. Baskaran, A. Baskaran, J. Lowengrub, Kinetic density functional theory of freezing, J. Chem. Phys. 141 (2014), 174506, https://doi.org/10.1063/1.4900499.

[55] G.I. Tóth, L. Gránásy, G. Tegze, Nonlinear hydrodynamic theory of crystallization, J. Phys. Condens. Matter 26 (2014), 055001, https://doi.org/10.1088/0953-8984/26/5/055001.

[56] V. Heinonen, C.V. Achim, J.M. Kosterlitz, S.-C. Ying, J. Lowengrub, T. Ala-Nissila, Consistent Hydrodynamics for Phase Field Crystals, Phys. Rev. Lett. 116 (2016), 024303, https://doi.org/10.1103/PhysRevLett.116.024303.

[57] A. Baskaran, Z. Guan, J. Lowengrub, Energy stable multigrid method for local and non-local hydrodynamic models for freezing, Comput. Methods Appl. Mech. Eng. 299 (2016) 22, https://doi.org/10.1016/j.cma.2015.10.011.

[58] S. Praetorius, A. Voigt, A navier-stokes phase-field crystal model for colloidal suspensions, J. Chem. Phys. 142 (15) (2015), 154904, https://doi.org/10.1063/1.4918559.

[59] F. Podmaniczky, G.I. Tóth, G. Tegze, L. Gránásy, Hydrodynamic Theory of Freezing: Nucleation and Polycrystalline Growth, Phys. Rev. E 95 (2017), 052801, https://doi.org/10.1103/PhysRevE.95.052801.

[60] F. Podmaniczky, L. Gránásy, Nucleation and post-nucleation growth in diffusion controlled and hydrodynamic theory of solidification, Crystals 11 (2021) 437, https://doi.org/10.3390/cryst11040437.

[61] S. Van Teeffelen, R. Backofen, A. Voigt, H. Löwen, Derivation of the Phase-Field-Crystal Model for Colloidal Solidification, Phys. Rev. E 79 (2009), 051404, https://doi.org/10.1103/PhysRevE.79.051404.

[62] T.V. Ramakrishnan, M. Yussouff, First-principles order-parameter theory of freezing, Phys. Rev. B 19 (1979) 2775, https://doi.org/10.1103/PhysRevB.19.2775.

[63] L.D. Landau, E.M. Lifshitz, Fluid Mechanics, Pergamon, New York, 1959.

[64] B.Z. Shang, N.K. Voulgarakis, J.-W. Chu, Fluctuating hydrodynamics for multiscale simulation of inhomogeneous fluids: Mapping all-atom molecular dynamics to

capillary waves, J. Chem. Phys. 135 (4) (2011), 044111, https://doi.org/10.1063/1.3615719.

[65] E.S. Kikkinides, P.A. Monson, Dynamic density functional theory with hydrodynamic interactions: Theoretical develop-ment and application in the study of phase separation in gas-liquid systems, J Chem Phys. 142 (2015), 094706, https://doi.org/10.1063/1.4913636.

[66] P. Stefanovic, M. Haataja, N. Provatas, Phase-Field Crystals with Elastic Interactions, Phys. Rev. Lett. 96 (2006), 225504, https://doi.org/10.1103/PhysRevLett.96.225504.

[67] P. Galenko, D. Danilov, V. Lebedev, Phase-Field-Crystal and Swift-Hohenberg Equations with Fast Dynamics, Phys. Rev. E 72 (2009), 051110, https://doi.org/10.1103/PhysRevE.79.051110.

[68] G. Tegze, G. Bansel, G.I. Tóth, T. Pusztai, Z. Fan, L. Gránásy, J. Comput. Phys. 228 (2009) 1612, https://doi.org/10.1016/j.jcp.2008.11.011.

[69] K.-A. Wu, A. Karma, Phase-Field Crystal Modeling of Equilibrium BCC-Liquid Interfaces, Phys. Rev. B 76 (2007), 184107, https://doi.org/10.1103/PhysRevB.76.184107.

[70] A. Jaatinen, C.V. Achim, K.R. Elder, T. Ala-Nissila, Thermodynamics of BCC Metals in Phase-Field-Crystal Models, Phys. Rev. E 80 (2009), 031602, https://doi.org/10.1103/PhysRevE.80.031602.

[71] J. Berry, K.R. Elder, M. Grant, Simulation of an Atomistic Dynamic Field Theory for Monatomic Liquids: Freezing and Glass Formation, Phys. Rev. E 77 (2008), 061506, https://doi.org/10.1103/PhysRevE.77.061506.

[72] G.I. Tóth, G. Tegze, T. Pusztai, G. Tóth, L. Gránásy, Polymorphism, crystal nucleation and growth in the phase-field crystal model in 2D and 3D, J. Phys.: Condens. 22 (Matter 2010,), 364101.

[73] V.V. Hoang, Molecular dynamics simulation of liquid and amorphous Fe nanoparticles, Nanotechnol 20 (29) (2009), 295703, https://doi.org/10.1088/0957-4484/20/29/295703.

[74] W. Lechner, C. Dellago, Accurate Determination of Crystal Structures Based on Averaged Local Bond Order Parameters, J. Chem. Phys. 129 (2008), 114707, https://doi.org/10.1063/1.2977970.

[75] P.M. Larsen, S. Schmidt, J. Schiøtz, Robust structural identification via polyhedral template matching, Modelling Simul. Mater. Sci. Eng. 24 (5) (2016), 055007, https://doi.org/10.1088/0965-0393/24/5/055007.

[76] OVITO: Open Visualization Tool. https://www.ovito.org/.

[77] K. Barkan, H. Diamant, R. Lifshitz, Stability of quasicrystals composed of soft isotropic particles, Phys. Rev. B 83 (2011), 172201, https://doi.org/10.1103/PhysRevB.83.172201.

[78] J. Rottler, M. Greenwood, B. Ziebarth, Morphology of monolayer films on quasicrystalline surfaces from the phase field crystal model, J. Phys.: Condens.

Matter 24 (13) (2012), 135002, https://doi.org/10.1088/0953-8984/24/13/135002.

[79] C.V. Achim, M. Schmiedeberg, H. Löwen, Growth Modes of Quasicrystals, Phys. Rev. Lett. 112 (2014), 255501, https://doi.org/10.1103/PhysRevLett.112.255501.

[80] P. Subramanian, A.J. Archer, E. Knobloch, A.M. Rucklidge, Three-Dimensional Icosahedral Phase Field Quasicrystal, Phys. Rev. Lett. 117 (2016), 075501, https://doi.org/10.1103/PhysRevLett.117.075501.

[81] M. Schmiedeberg, C.V. Achim, J. Hielscher, S.C. Kapfer, H. Löwen, Dislocation-free growth of quasicrystals from two seeds due to additional phasonic degrees of freedom, Phys. Rev. E 96 (2017), 012602, https://doi.org/10.1103/PhysRevE.96.012602.

[82] P. Hirvonen, G.M. La Boissonière, Z. Fan, C.V. Achim, N. Provatas, K.R. Elder, T. Ala-Nissila, Grain extraction and microstructural analysis method for two-dimensional poly and quasicrystalline solids, Phys. Rev. Mater. 2 (2018), 103603, https://doi.org/10.1103/PhysRevMaterials.2.103603.

[83] S. Tang, Z. Wang, J. Wang, K. Jiang, C. Liang, Y. Ma, W. Liu, Y. Du, An atomic scale study of two-dimensional quasicrystal nucleation controlled by multiple length scale interactions, Soft Matter 16 (24) (2020) 5718–5726, https://doi.org/10.1039/C9SM02243K.

[84] C. Liang, K. Jiang, S. Tang, J. Wang, Y. Ma, W. Liu, Y. Du, Molecular-level insights into the nucleation mechanism of one-component soft matter icosahedral quasicrystal studied by phase-field crystal simulations, Cryst. Growth Des. 22 (4) (2022) 2637–2643, https://doi.org/10.1021/acs.cgd.2c00074.

[85] C. Hu, R. Wang, W. Yang, D. Ding, Point Groups and Elastic Properties of Two-Dimensional Quasicrystals, Acta Cryst. A 52 (1996) 251, https://doi.org/10.1107/S0108767395014036.

[86] S.E. Burkov, Are layered two-dimensional quasicrystals periodic in the third direction? J. Stat. Phys. 65 (1–2) (1991) 395–401, https://doi.org/10.1007/BF01329868.

[87] M. Dzugutov, S.I. Simdyakin, F.H.M. Zetterling, Decoupling of Diffusion from Structural Relaxation and Spatial Heterogeneity in a Supercooled Simple Liquid, Phy. Rev. Lett. 89 (2002), 195701, https://doi.org/10.1103/PhysRevLett.89.195701.

[88] M. Elenius, T. Oppelstrup, M. Dzugutov, Evidence for a simple monatomic ideal glass former: The thermodynamic glass transition from a stable liquid phase, J. Chem. Phys. 133 (17) (2010), 174502, https://doi.org/10.1063/1.3493456.

[89] G. Kurtuldu, A. Sicco, M. Rappaz, Icosahedral quasicrystal-enhanced nucleation of the fcc phase in liquid gold alloys, Acta Mater. 70 (2014) 240, https://doi.org/10.1016/j.actamat.2014.02.037.